Can. J. Remote Sensing, Vol. 34, No. 2, pp. 143–158, 2008

Riparian marshland composition and biomass mapping using Ikonos imagery

Kristie A. Dillabaugh and Douglas J. King

Abstract. The Ontario Wetland Evaluation System (OWES) employs mostly field-based visual assessments of wetland extent, composition, and productivity as primary indicators in determining which wetlands should be considered provincially significant and protected. A given wetland is generally assigned single attributes that are assumed to represent the whole wetland extent. High spatial resolution satellite remote sensing offers potential to map and monitor spatial variability of given attributes within a wetland. In this study, Ikonos imagery was used to map vegetation composition and biomass in three riparian marshes near Ottawa, Ontario. For vegetation composition mapping, separability and correlation analyses aided the selection of an optimum set of spectral and texture input variables. Several maximum likelihood classification tests for sets of terrestrial and aquatic vegetation classes gave best accuracies from 61% for seven classes to 88% for five classes. As an alternative, neural network classification was tested using various configurations of input variables and data. However, the best results did not match those from the maximum likelihood classification. For biomass mapping, dried green and senescent biomass collected at 75 locations were modelled using stepwise forward multiple regression. The best model produced was the logarithm of green biomass against a combination of texture and spectral variables (R^2 = 0.61). It was applied to the image data to map green biomass with an absolute error of 213 g/m^2, or approximately 40% of the mean field-measured biomass. Based on this error magnitude, the output map was aggregated into three classes of biomass (high, medium, and low) that showed a strong visual correspondence with the spatial distributions observed in the field. These results indicate strong potential for monitoring of vegetation composition and biomass changes within wetlands which may contribute to improvement of wetlands evaluation and monitoring in Ontario.

Résumé. Le système OWES (« Ontario Wetland Evaluation System ») utilise surtout des évaluations visuelles réalisées sur le terrain de l'étendue, de la composition et de la productivité des milieux humides comme indicateurs primaires pour déterminer lesquels des milieux humides devraient être considérés comme significatifs et devant être protégés au niveau provincial. On assigne généralement à un milieu humide donné des attributs uniques qui sont considérés comme représentatifs de l'ensemble du milieu humide. La télédétection satellitaire à haute résolution offre un bon potentiel pour la cartographie et le suivi de la variabilité spatiale d'attributs donnés à l'intérieur d'un milieu humide. Dans cette étude, on utilise des images d'Ikonos pour cartographier la composition de la végétation et la biomasse dans trois marécages riverains près d'Ottawa, en Ontario. Pour la cartographie de la composition de la végétation, des analyses de séparabilité et de corrélation ont aidé à la sélection d'un ensemble optimal de variables spectrales et de texture d'entrée. Plusieurs tests de classification par maximum de vraisemblance appliqués à des ensembles de classes de végétation terrestre et aquatique ont donné les meilleures précisions, variant de 61 % pour sept classes à 88 % pour cinq classes. Comme alternative, la classification par réseau de neurones a été testée en utilisant diverses configurations de variables d'entrée et de données. Toutefois, les meilleurs résultats n'ont pas été comparables à ceux de la classification par maximum de vraisemblance. Pour la cartographie de la biomasse, des échantillons de biomasse verte et sénescente séchée collectés sur 75 sites ont été modélisés à l'aide d'une régression multiple séquentielle (« stepwise forward »). Le meilleur modèle produit a été celui du log de la biomasse verte par rapport à une combinaison de variables spectrales et de texture (R^2 = 0,61). Il a été appliqué aux données images pour cartographier la biomasse verte avec une erreur absolue de 213 g/m^2 ou approximativement 40 % de la biomasse moyenne mesurée sur le terrain. Basé sur l'amplitude de cette erreur, la carte de sortie a été regroupée en fonction de trois classes de biomasse (élevée, moyenne et faible) et celle-ci affichait une correspondance visuelle forte avec les distributions spatiales observées sur le terrain. Ces résultats démontrent un fort potentiel pour le suivi de la composition de la végétation et des changements de la biomasse à l'intérieur des milieux humides susceptible de contribuer à l'amélioration de l'évaluation et du suivi des milieux humides en Ontario.
[Traduit par la Rédaction]

Received 8 August 2007. Accepted 1 February 2008. Published on the *Canadian Journal of Remote Sensing* Web site at http://pubs.nrc-cnrc.gc.ca/cjrs on 25 July 2008.

K.A. Dillabaugh and D.J. King.[1] Geomatics and Landscape Ecology Laboratory, Department of Geography and Environmental Studies, Carleton University, 1125 Colonel By Drive, Ottawa, ON K1S 5B6, Canada.

[1]Corresponding author (e-mail: Doug_king@carleton.ca).

Introduction

Wetlands are transitional zones located between terrestrial and aquatic ecosystems which experience seasonal or permanent above-surface water (Twolan-Strutt, 1995). As a result, saturated soils and hydrophytic vegetation predominate. Wetlands and wetland vegetation provide many environmental functions such as conversion of inorganic carbon to organic compounds through photosynthesis, circulation of essential nutrients such as phosphorus and nitrogen, absorption of water during wet periods and recharge of groundwater during drier periods, removal of sediments and debris from the water and absorption of pollutants, and provision of habitat for many plant and animal species (Twolan-Strutt, 1995; Mitsch and Gosselink, 2000; Larson and Newton, 1981; Lewis, 2001; Williams, 1990; Hammer, 1997).

Riparian wetlands are greatly influenced by adjacent rivers or streams and are therefore typically linear in form, processing large fluxes of energy and materials from upstream systems (Mitsch and Gosselink, 2000). Riparian marsh wetlands are nutrient-rich areas and are particularly important for increasing riparian habitat and stabilizing riverbanks (Hammer, 1997). The preservation of shoreline vegetation and wetlands is critical for maintaining the health and biodiversity of a river.

Vegetation plays a key ecological role within wetland environments. In marshes, the dominant vegetation types are emergents and aquatics, although peripheral trees and low shrubs are often present (Cronk and Fennessy, 2001). In Ontario, due to increased pressures on wetlands from urbanization and agriculture, it became necessary to develop protection policies, which in turn led to the development of an evaluation system in the early 1980s to identify priority wetlands for protection. The purpose of the Ontario Wetland Evaluation System (OWES) developed by the Ontario Ministry of Natural Resources (OMNR, 1993) is to rate the potential significance of a wetland based on four components: hydrology, biology, social benefits, and special features. The assessment of wetlands by the OWES is conducted on the ground with the aid of air photographs and existing maps. These methods may introduce observer bias, as subjective scoring is required and the nearly horizontal viewing perspective may result in missed features or error in assessment of characteristics that are far from view. This field-based assessment is labour intensive and expensive for large wetlands, allowing only a few sample observation locations. Access to wetland environments is also difficult because of uneven and unstable terrain, tall dense vegetation, mud, and water. The end result of the assessment process is a set of aggregated attributes for a delineated wetland that is assumed to represent the whole wetland area. There is no means within this evaluation system to map the spatial distribution of vegetation type or quantity within a given wetland unless subareas are specifically delineated and described by the assessor. Currently, efforts are underway to revise the OWES to include more geospatial data, including data derived from remote sensing.

The goal of this research was to determine if high spatial resolution satellite remote sensing could be effective in mapping vegetation type and biomass within riparian marsh wetlands. It has been known for some time that remote sensing can be used to identify wetland type, extent, spatially associated resources, and vegetation communities (Lyon and McCarthy, 1995). Image-based methods are well suited to spatiotemporal monitoring of wetlands because they can be standardized, alleviating the subjectivity caused by differences between field observers. Satellite images also provide an effective visual and quantitative archive of conditions within a wetland at a given time that can be used in temporal change analysis more effectively than the aggregated data from field assessment.

Past research has been mostly conducted at moderate scales using sensors such as Landsat to detect wetland occurrence and classify wetlands into broad classes such as marshes, swamps, fens, or bogs (e.g., Herr and Queen, 1993; Rogers and Kearney, 2003). The primary goal of these types of studies is to inventory wetland area and type, in a regional context, for a variety of ecological and environmental process applications. Little research has been conducted on the potential of high-resolution imagery for characterization of within-wetland vegetation patterns. Of that research, most has been conducted with airborne imagery. For example, Jensen et al. (1984) used four-band airborne multispectral scanner data with 2.8 m pixels to map six classes of nontidal wetland vegetation with an overall accuracy of 83.5%. Classes that were spectrally similar included persistent emergent, nonpersistent emergent, scrub–shrub, and mixed deciduous forest. Using hyperspectral 1 m pixel compact airborne spectrographic imager (*casi*) imagery, Green et al. (1998) mapped nine detailed mangrove classes with a higher overall accuracy (85%) than could be achieved with Landsat and SPOT imagery. Using 2.5 m pixel casi imagery, Thomson et al. (2004) classified intertidal salt marsh in the Netherlands into 15 classes with accuracies of 75.8% and 60.6% for 1998 and 2000 data, respectively. Spectral overlap occurred between spatially adjacent classes and between classes within the tidal shore gradient. Very few studies have been conducted in terms of evaluating high-resolution satellite imagery. One example is that of Dechka et al. (2002) where May and July Ikonos panchromatic images (1 m pixels) were fused with multispectral (4 m pixels) imagery to analyze the separability of wetland and upland classes using spectral and textural data. A nine-class map was produced with an overall accuracy of 47%. Classes were then aggregated according to the dominant vegetation communities. Another example is that of Olmanson et al. (2002), who used pan-sharpened multispectral Ikonos imagery to map three classes of emergent aquatic vegetation and four classes of submerged vegetation.

The aforementioned studies illustrate the potential for high-resolution imagery in mapping the spatial distribution of vegetation types within given wetlands. The first objective of this research was to conduct such an assessment in a wetland environment different from those which had been previously studied, namely riparian marshes. The second objective, which has not been previously attempted, was to determine if wetland

productivity in terms of green and senescent aquatic and terrestrial biomass could be modelled and mapped in such marshes. Lastly, as most other studies have only analyzed spectral data for wetland mapping, a third objective was set to evaluate image texture in high-resolution imagery as a representation of spatial heterogeneity in surface reflectance that has potential for vegetation type and biomass discrimination.

Methods

Study area and field data acquisition

The study area encompasses 101 km^2 and focusses on three riparian marsh wetlands along the Rideau River in eastern Ontario: Barbers Creek, Irish Creek, and Kilmarnock (**Figure 1**). Parts of the edges of these wetlands were accessible by road, and the interior areas were more accessible by water. All are single, contiguous riparian wetland areas that have been evaluated by the OMNR for potential wetland significance. Barbers Creek wetland received provincial significance status because it is regionally significant for waterfowl staging and locally significant for waterfowl production, particularly for colonial waterbirds or localized species populations such as the great blue heron (*Ardea herodias).* Irish Creek wetland received provincial significance status as a regionally significant waterfowl staging area and an important spawning ground for northern pike (*Esox lucius*). The OMNR has observed species at risk, such as the least bittern (*Ixobrychus*

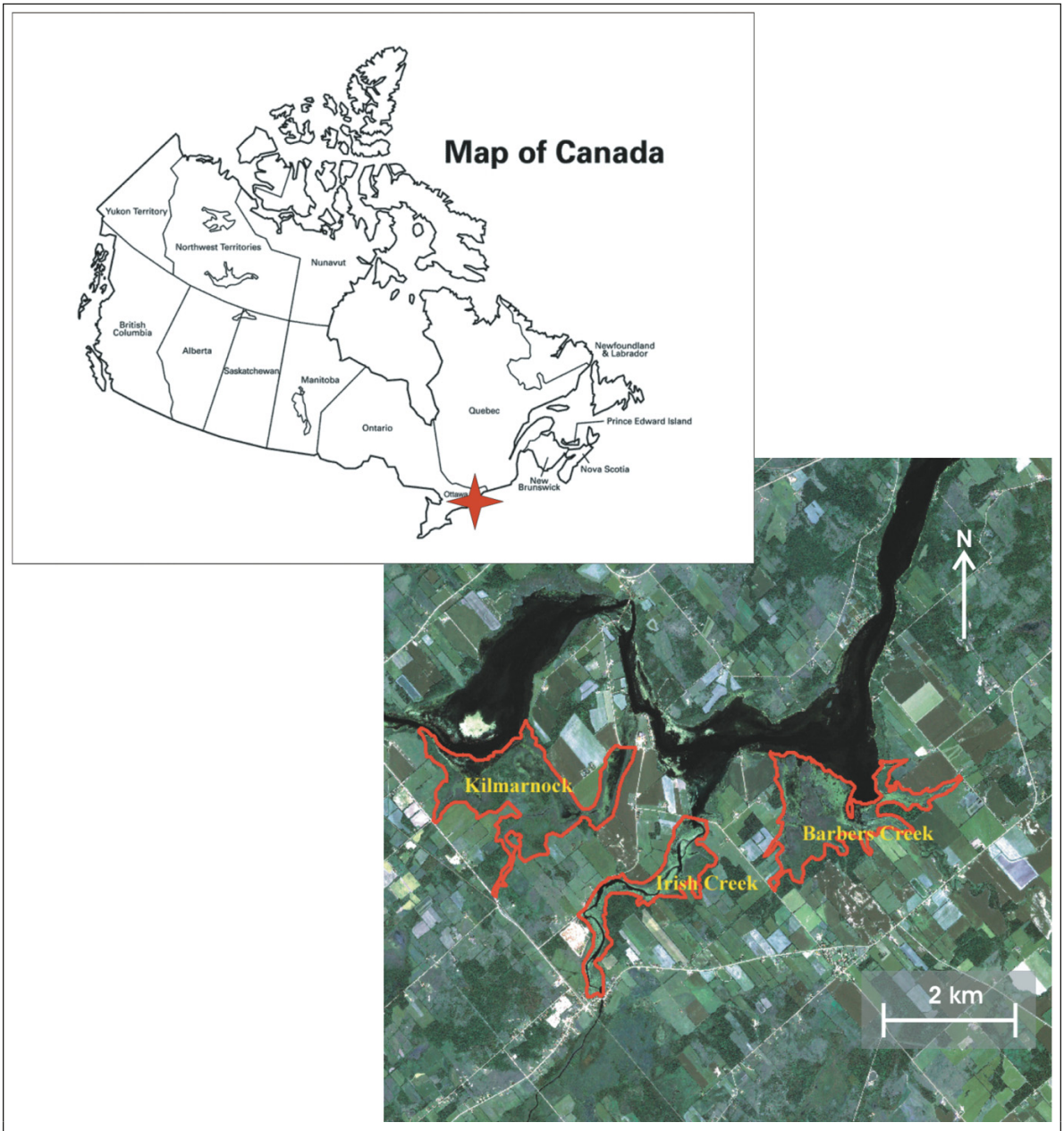

Figure 1. Kilmarnock, Irish Creek, and Barbers Creek wetlands delineated on August 2003 Ikonos imagery.

Table 1. The seven vegetation classes and the dominant species and number of field samples in each class.

Class	Dominant vegetation	No. of samples
Emergent terrestrial (EM)	Common cattail (*Typha latifolia*); purple loosestrife (*Lythrum salicaria*); spotted joe-pye-weed (*Eupatorium maculatum*); swamp milkweed (*Asclepias incarnata*); meadow horsetail (*Equisetum pratense*)	45
Shrub (SHR)	Speckled alder (*Alnus incana*); slender willow (*Salix petiolaris*); sweet gale (*Myrica gale*); red osier dogwood (*Cornus stolonifera*)	27
Grasses–sedges (GS)	Cyperus-like sedge (*Carex pseudo-cyperus*); green sedge (*Carex viridula*)	5
Floating aquatic (FLAQ)	Yellow pond lily (*Nuphar variegatum*); fragrant white water lily (*Nymphaea odorata*); floating-leaved pondweed (*Potamogeton natans*)	9
Emergent aquatic (EMAQ)	Common reed (*Phragmites australis*); stiff arrowhead (*Sagittaria rigida*); pickerelweed (*Pontederia cordata*); large-fruited burreed (*Sparganium eurycarpum*)	5
Forest (FOR)	Black ash (*Fraxinus nigra*); sugar maple (*Acer saccharum*)	5
Open water (OW)	No vegetation	11

exilis), and the black tern (*Chlidonias niger*), a species protected under the *Migratory Birds Convention Act* (Gerson, 1988; Austen et al., 1994), was observed during the fieldwork for this research. Kilmarnock marsh was not evaluated as provincially significant but has been identified as an important waterfowl staging area.

Field data were collected in August 2003 during the time of peak productivity. For classification of vegetation composition, 107 locations were selected based on the following criteria: maximized separation between locations to minimize spatial autocorrelation when using the data as samples in statistical analyses; homogeneous species composition and structure, which were visually assessed, over an area of at least 12 m × 12 m, equivalent to about 3 × 3 Ikonos multispectral pixels; accessibility by road or water; and representation of the full range of vegetation cover within the wetlands. For the first criterion, a minimum separation of about 200 m was used as a balance between (*i*) the desired number of locations to provide adequate training and validation sample sizes and the possible spacing between locations in relation to the wetland sizes and (*ii*) ease of access to sample locations. The exact figure of 200 m was selected somewhat arbitrarily in terms of spatial autocorrelation, which has not yet been studied for the image and field data of these wetlands. However, it was expected that this minimum spacing criterion would reduce spatial autocorrelation compared with lesser separation distances. The coordinates of each location were recorded using a professional-quality, real-time differential global positioning system (GPS) with consistent submetre accuracy (Trimble Navigation Ltd., available from www.trimble.com). At each location, the vegetation was classified as one of emergent terrestrial (EM), shrub (SHR), grasses–sedges (GS), floating aquatic (FLAQ), emergent aquatic (EMAQ), forest (FOR), and open water (OW). The vegetation classes are an aggregated version of those used by the OMNR for evaluating wetlands. **Table 1** lists the seven classes, the species that dominate each class, and class sample size.

For biomass modelling, a subset of 75 of these locations was selected based on accessibility. Following Ikonos image acquisition, at each location, a 1 m × 1 m wooden frame was placed over the vegetation (**Figure 2**) near the centre of the "homogeneous" sample area (of about 12 m × 12 m as stated previously). It was not feasible to sample and measure larger areas of biomass at each location and maintain an adequate sample size for statistical analysis. Thus, regression modelling of biomass using 1 m × 1 m samples versus 4 m × 4 m Ikonos pixel data (see later in the Methods section) was expected to include some noise from this mismatch of sample areas. The vegetative species within the frame were identified, average vegetation height was measured for the terrestrial samples, and percent cover was visually estimated. A digital camera was used to acquire vertically downward colour photographs of each plot. Following image acquisition, vegetation within the frame was then clipped, bagged, and transported back to the laboratory. All above-ground vegetation was clipped for the terrestrial samples, and all vegetation above the water surface and submerged vegetation to a depth of 10 cm were clipped for the aquatic samples. Vegetation was stored in a refrigerator (0–5 °C) until the plants were chopped and oven-dried at 105 °C for 24 h. Drying curves of mass versus time were generated in tests, and 24 h was found to be the minimum time required for complete drying. Green and senescent (yellow) vegetation were weighed separately for stratified modelling. The biomass measurement and image modelling portion of this research represents a unique contribution because this process of clipping, transport, storage, drying, and weighing of biomass is rarely attempted outside short vegetation dryland studies. It was very difficult to conduct the study in these wetlands where water depth and mud were often waist deep, and where canoe access to certain sites was very time-consuming and arduous.

Image acquisition and processing

Ikonos multispectral and panchromatic cloud-free imagery were acquired on 25 August 2003. The image provider performed a standard geometric correction of the raw image data and resampled the image to the universal transverse Mercator (UTM) (zone 18, NAD83 datum) projection using cubic convolution interpolation. PCI Geomatica version 9.1

Figure 2. Example photographs of terrestrial plot (a) and aquatic plot (b).

was used for all image processing. The multispectral and panchromatic imagery was georeferenced more precisely using 17 ground control points (GCPs) at intersecting roadways and other landmark features, whose positions were measured using the differential GPS. A first-order polynomial affine transformation and nearest neighbour resampling were used, with root mean square errors (RMSEs) of [0.05(x), 0.05(y)] and [0.14(x), 0.13(y)] pixels for the multispectral and panchromatic images, respectively. The multispectral RMSE of 0.05 pixels is equivalent to about 0.2 m. Given the GCPs were spread throughout the 10 km × 10 km image with an average spacing of about 2 km, that the terrain was very flat, and that the GCPs were very well identified in the field, it was deemed that plot locations occurring between GCPs would not have georeferencing errors in excess of 1–2 m (i.e., 5–10 times the affine transformation RMSE). This provided confidence that the sample location coordinates could be associated with individual 4 m × 4 m pixels in the georeferenced imagery. A wetland mask was manually delineated, and various data layers were derived from the imagery, including texture measures and vegetation indices.

Eight co-occurrence texture measures (homogeneity, contrast, dissimilarity, mean, variance, entropy, angular second moment, correlation) and four grey level difference vectors (GLDV angular second moment, GLDV entropy, GLDV mean, and GLDV contrast (Haralick et al., 1973)) were extracted from the green and near-infrared (NIR) spectral bands using two moving window sizes, namely 3 × 3 and 5 × 5. These spectral bands were selected for texture analysis because of their visibly greater spatial detail and because they were not highly correlated with each other (r = 0.62). The window sizes were selected to represent local texture. Larger windows produce more stable probability density functions from which the textures are calculated, but with sample areas being selected to be homogeneous over a minimum area of nine to 25 pixels, it was not prudent to exceed a 5 × 5 window size. These co-occurrence texture measures produce output images of 32-bit real numbers for each pixel that were scaled to 16-bit to match the bit rate of the spectral data. Each texture image is comprised of graded pixel values, with bright areas representing high-frequency spatial variation and dark areas representing more spatially uniform surface reflectance (or vice versa for some measures). The panchromatic Ikonos image with 1 m pixels was not used to derive texture measures because the file size produced was much too unwieldy for all the tests of separability, classification, and regression as described later in the paper. At 16 times the file size of a multispectral band, extraction of twelve 32-bit texture images and resampling all the multispectral variables (four spectral bands and six vegetation indices (see later in the paper)) down to 1 m pixels would have produced a dataset that could not be processed in a reasonable time to conduct the multitude of tests desired.

The vegetation indices included atmospheric and soil vegetation index (ASVI), differenced vegetation index (DVI), modified soil adjusted vegetation index (MSAVI), normalized difference vegetation index (NDVI), ratio vegetation index (RVI), soil adjusted vegetation index (SAVI) using L = 0.5 (Heute, 1988), and transformed vegetation index (TVI) (as defined in Bannari et al., 1995; Eastwood et al., 1997; Ozesmi and Bauer, 2002; Tan et al., 2003). Some of these are "soil-adjusted" indices that were selected because the marshes included significant amounts of yellow senescent vegetation and smaller amounts of visible soil.

Wetland vegetation classification

Once the image dataset was complete, training data were generated for the 3 × 3 pixel window at each of the 107 locations where vegetation had been field-classified. All spectral and texture variables were found to be normally

Table 2. Neural network configurations.

Neural network number	Inputs	Momentum rate	Learning rate	Maximum no. of iterations
1	Spectral bands plus A2M5grn and CON5nir	0.9	0.1	1 000
2	Spectral bands, A2M5grn, and CON5nir plus MSAVI, NDVI, RVI, SAVI, and TVI	0.9	0.1	1 000
3	Spectral bands, A2M5grn, and CON5nir plus MSAVI, NDVI, RVI, SAVI, and TVI	0.6	0.2	1 000
4	Spectral bands plus A2M5grn and CON5nir	0.9	0.9	1 000
5	Spectral bands plus A2M5grn and CON5nir	0.9	0.1	25 000
6	Spectral bands plus A2M5grn and CON5nir	0.9	0.1	100 000
7	Spectral bands plus A2M5grn and CON5nir	0.9	0.1	100 000
8	Spectral bands plus A2M5grn and CON5nir	0.9	0.1	250 000
9	Spectral bands, A2M5grn, and CON5nir plus MSAVI, NDVI, RVI, SAVI, and TVI	0.9	0.1	100 000

distributed, with only slight skewness noted for some texture measures. To determine the best texture measures for class discrimination, separability analyses using the Bhattacharya distance (Jensen, 2005) and the training data for the seven classes listed previously were conducted for 12 sets of input variables, each comprising the four spectral bands plus one of the 12 texture measures. The best two textures (see the Results section) were then combined with the four spectral bands and (or) individual vegetation indices in additional separability analyses. These analyses were conducted for varied numbers of classes: (*i*) all seven classes in **Table 1**; (*ii*) a six-class set with the EM and SHR classes merged (due to poor discrimination; see the Results section); and (*iii*) a five-class set with the EM, SHR, and GS classes merged into a terrestrial marsh (TERm) class due to poor discrimination. The sets of input variables that resulted in the highest separability (there were several sets with similar results) were then used in classification tests.

For classification, the 107 locations of field and image data were randomly divided into equal training and validation datasets. Maximum likelihood classification (MLC) was selected as the main classifier to test because it is a standard that is well known and results can be easily judged by the broader remote sensing and wetlands scientific communities. In addition, given potential revision of the OWES procedures, this classifier serves as a straightforward means that can be immediately adopted in operational testing. It was conducted using probability density function bounds of three standard deviations and equal a priori probabilities for all classes, as their expected relative proportions were not known. Classification tests were conducted for the sets of seven, six, and five classes listed previously. A 3 × 3 mode filter was applied to the output maps to reduce individual pixel noise. Accuracy was assessed using a standard error matrix (Congalton, 1991) and K_{hat} statistic (Rosenfield and Fitzpatrick-Lins, 1986). Due to small numbers of sample sites for some classes, 3 × 3 validation windows were used. The pixels within each 3 × 3 window were obviously autocorrelated, but because of restricted accessibility, it was not feasible to visit enough individual sample pixel locations to develop a validation dataset with adequate independent sample numbers for all classes.

In addition to MLC, a feed-forward, back-propagation neural network classifier (Rumelhart et al., 1986) was implemented as an alternative because it is not constrained by the number of input variables or normal data distribution requirements. The networks were trained using the five wetland class set mentioned previously for initial tests. If accuracy was higher than that for the MLC, further tests with the six- and seven-class sets were planned. Several tests were performed changing the number of iterations, the momentum and learning rates, and the input variables (**Table 2**) to try to achieve convergence towards acceptable limits for individual class and total errors and to improve classification accuracy. PCI Geomatics (2004) suggests that a small learning rate (e.g., 0.1) reduces the risk of oscillation and nonconvergence of the training data. A learning rate of 0.1 and a momentum rate of 0.9 were used in most tests based on common results from the literature (e.g., Foody et al., 1996; Pierce et al., 1994). In neural network 3, momentum and learning rates were used as recommended by Kavzoglu and Mather (2003) from comparisons of many configurations of network parameters for two datasets. In some tests, the number of iterations was increased while keeping other parameters constant to try to obtain convergence of the network. Spectral and textural data producing the best results from the MLC were used as inputs in many of the networks to make direct comparisons with the MLC results. Additionally, for some configurations, vegetation indices were included as inputs to determine if they produced higher classification accuracies. The sample sites and data used for the MLC were also used for training and validation.

Biomass modelling

All the raw band, vegetation index, and texture variables listed previously were extracted for the single pixel at each biomass field plot location. Forward stepwise regression of these image variables against dry biomass was conducted. Probabilities to enter and remove were set at 0.05 and 0.10, respectively. Scatterplots were analyzed to evaluate linearity, which revealed nonlinear relationships between many of the independent image variables and the dependent biomass variable. In addition, the biomass data were non-normal, with a general trend of decreasing numbers of plots as biomass

Table 3. Stratified biomass datasets used in regression analysis, with sample size (n) in parentheses.

Terrestrial and aquatic (n = 75)	Terrestrial (n = 54)	Aquatic (n = 21)
Green biomass	Green biomass	Green biomass
Green and senescent biomass combined	Green and senescent biomass combined	
Senescent biomass	Senescent biomass	

increased. As a result, logarithm transformation of biomass was conducted, and models were compared to those derived from nontransformed data. Multicollinearity was reduced using only image variables that were not highly correlated with each other as inputs ($r < 0.80$). Once the best model was created, the variance inflation factor VIF = $1/(1 - R^2)$ given for each independent variable was checked to ensure that it was below the desired threshold limit from the VIF equation (Allison, 1999; Freund and Wilson, 1998). Modelling was conducted using the whole dataset and data stratified into terrestrial (n = 54) and aquatic (n = 21) classes and green versus senescent vegetation as shown in **Table 3**. Further stratification into more precise classes was not possible due to limited sample numbers.

Model performance was evaluated based on the adjusted coefficient of determination (R^2_{adj}) for the model, the R^2 change produced by each variable, the standard error of estimate (S_e), the significance (p) value for each entered variable, and the number of variables entered into the model based on the 1:10 variable to sample ratio rule (Stevens, 1996). Model residuals were checked for uniformity and normality. From the tests of **Table 3**, five separate model runs were conducted for the biomass variable that was best modelled, randomly splitting the sample data into 70% training and 30% validation, to determine the average and variability in R^2, S_e, mean prediction error, mean absolute prediction error, and prediction RMSE.

As the green band 5 × 5 mean texture measure dominated almost all models (see the Results section), an additional validation analysis was conducted for five models created with the same 70% training and 30% validation being randomly split and a constraint of allowing only one variable to enter. This was intended to determine whether a single-variable model could be as effective at estimating biomass as a multiple-variable model.

Results

Wetland vegetation classification

Separability analysis

Separability analyses for each of the 12 texture measures (when combined individually with the four spectral bands) showed angular second moment derived from a 5 × 5 window in the green band (A2M5grn) and contrast derived from a 5 × 5 window in the NIR band (CON5nir) to be better than the other texture measures in terms of minimum and mean separability among class pairs for the seven-class set. Angular second moment (A2M) measures the degree of orderliness in a sample window by summing the probabilities of all pairs of adjacent pixel values. If certain pairs of values are more frequent, the data in the window are more orderly and texture is lower, leading to a higher A2M value. Contrast measures the summed probability of pairs of pixel values in the window weighted by the square of their differences. It is therefore very high where spatial frequency is high, i.e., where edges are present in the image. These two textures are representative of the broader complementary texture groups orderliness and contrast (Hall-Beyer, 2007). In general, the floating aquatic and forest classes had higher texture for both measures than the other classes, which consisted of vertical grass, sedge, and shrub types of vegetation. Open water, as expected, had the lowest texture.

Both A2M5grn and CON5nir were not correlated with either the spectral bands or the vegetation indices ($r < 0.32$). **Table 4** shows the separability results when these two textures were combined with the four spectral bands for all seven classes, six classes with emergent terrestrial and shrub merged, and five classes with grasses–sedges merged into the emergent terrestrial and shrub class to form a general terrestrial marsh class. For seven classes, the average separability was lower than that commonly used to indicate good potential for class discrimination (1.7–1.9 as defined by Jensen, 2005), but separability increased as classes were merged. Separability results for input data consisting of a vegetation index and the two texture measures were similar to those listed in **Table 4**. Thus, the vegetation indices were retained for classification tests in input set combinations with the texture measures and spectral bands.

Classification results

As expected, the MLC results showed that overall accuracy significantly improved as classes were merged, with the highest accuracy obtained using five classes, as was observed in the separability analysis. For the seven-, six-, and five-class tests of combinations of input variables, the best accuracies were obtained using one vegetation index (either MSAVI or TVI) combined with the visible bands and the A2M5grn and CON5nir textures. Overall accuracy was 61.3%, 71.6%, and 87.8%, respectively. Error matrices for the best seven- and six-class maps are shown in **Tables 5** and **6**. **Figure 3** shows the best five-class map, with its corresponding error matrix in **Table 7**. Note that through class merging, the terrestrial marsh class in **Table 7** ended up having many more samples than the other classes, thus weighting the overall accuracy.

Despite poor classification of the emergent aquatic class, it was not merged with the floating aquatic class, as the two classes were structurally very dissimilar (see **Figure 4**) and its confusion was more with the terrestrial marsh class (evident in comparing **Figure 4a** with **Figure 2a**). Both had similar vegetation structure, with emergent aquatic being dominated by common reed and terrestrial marsh by common cattail, where each species consists of mostly erect flat leaves and forms large, dense colonies.

However, even though none of the validation samples for emergent aquatic were classified correctly (**Tables 5–7**), the

Table 4. Training data separability (Bhattacharrya distance) for varying numbers of wetland classes and the best input variables comprising the four spectral bands, A2M5grn, and CON5nir.

Wetland classes used during classification	Minimum separability	Average separability	Class pair with minimum separability
Seven classes	0.68	1.68	Emergent terrestrial and shrub
Six classes; emergent terrestrial and shrub merged	1.22	1.87	Emergent terrestrial and shrub and grasses–sedges
Five classes; emergent terrestrial and shrub and grasses–sedges merged into terrestrial marsh	1.63	1.91	Terrestrial marsh and emergent aquatic

Table 5. Classification error matrix showing validation pixel numbers, producer's accuracy, and user's accuracy for seven classes, in which rows are reference data and columns are classified data (K_{hat} = 0.47).

	EM	SHR	FLAQ	EMAQ	OW	FOR	GS	Total	Producer's accuracy (%)
EM	155	21	6	16	0	0	0	198	78.3
SHR	30	51	0	23	0	8	5	117	43.6
FLAQ	0	0	36	0	0	0	0	36	100.0
EMAQ	7	8	0	0	0	0	3	18	0.0
OW	0	0	0	0	45	0	0	45	100.0
FOR	0	23	0	0	0	0	4	27	0.0
GS	25	0	2	0	0	0	0	27	0.0
Total	217	103	44	39	45	8	12	468	
User's accuracy (%)	71.4	49.5	81.8	0.0	100.0	0.0	0.0		

Table 6. Classification error matrix showing validation pixel numbers, producer's accuracy, and user's accuracy for six classes, in which rows are reference data and columns are classified data (K_{hat} = 0.44).

	EM/SHR	FLAQ	EMAQ	OW	FOR	GS	Total	Producer's accuracy (%)
EM/SHR	262	6	37	0	7	3	315	83.2
FLAQ	0	36	0	0	0	0	36	100.0
EMAQ	16	0	0	0	0	2	18	0.0
OW	8	0	0	37	0	0	45	82.2
FOR	21	0	1	0	0	5	27	0.0
GS	23	4	0	0	0	0	27	0.0
Total	330	46	38	37	7	10	468	
User's accuracy (%)	79.4	78.3	0.0	100.0	0.0	0.0		

Note: Emergent terrestrial and shrub classes were merged.

locations of the pixels assigned to this class, shown in red in **Figure 3**, corresponded well with the locations in which this vegetation class was observed in the field, i.e., generally in aquatic nearshore areas and adjacent to floating aquatic vegetation.

In neural network classification tests, none of the nine networks fully converged to achieve both the maximum allowable individual class (0.001) and total (0.01) errors. The smallest individual error was achieved by neural network 9, which did not converge even after 100 000 iterations. Overall classification accuracies were generally lower for the neural networks compared with those from the MLC using the same five wetland classes. Neural network 9 achieved the highest overall accuracy of 84.4% and a K_{hat} statistic of 0.64. **Table 8** shows the corresponding error matrix. As for the corresponding MLC results (**Table 7**), the emergent aquatic class (EMAQ) was completely confused with terrestrial marsh. In addition, forest was classified with much poorer accuracy, being confused almost entirely with terrestrial marsh. The other three classes (TERm, FLAQ, and OW) showed some slightly better user's accuracies but also slightly poorer producer's accuracies than those from the MLC. Based on these poorer results and the effort required to test and adjust various network parameters, it was decided to not pursue further evaluation of neural networks for classification of these wetlands with these data.

Biomass modelling

Stepwise regression created statistically significant models ($p \leq 0.05$) for many of the biomass datasets (combinations of senescent + green vegetation for both aquatic and terrestrial environments). For brevity, the details of all of these models are not presented in tables, but a summary of pertinent statistical characteristics is given, followed by a table and equation showing details of the best model produced. Combined aquatic and terrestrial biomass data produced much stronger models

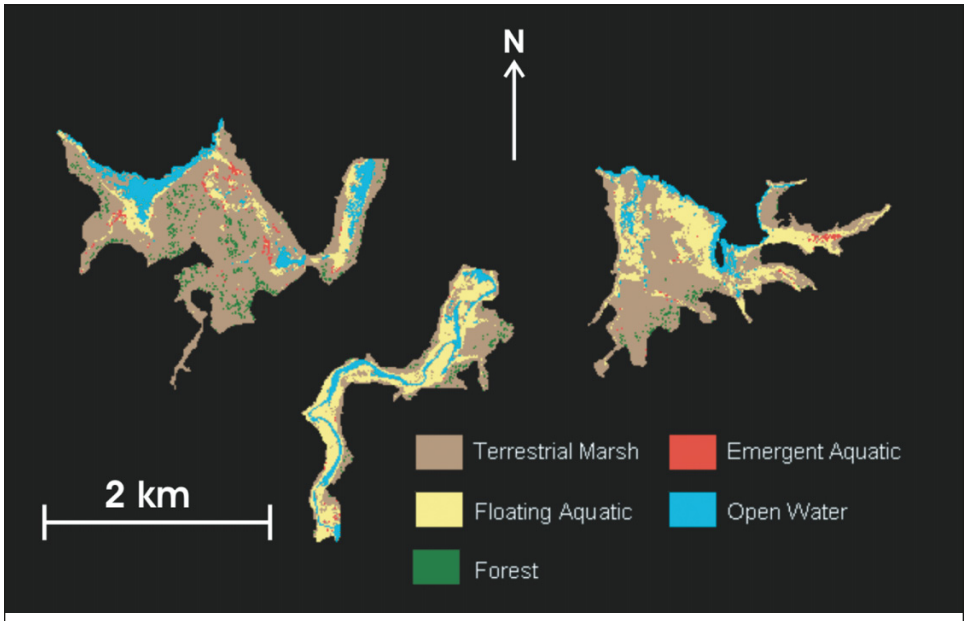

Figure 3. The most accurate five-class map derived using inputs of TVI vegetation index; blue, green, and red spectral bands; angular second moment 5 × 5 green band texture; and contrast 5 × 5 near-infrared band texture.

Table 7. Classification error matrix showing validation pixel numbers, producer's accuracy, and user's accuracy for five classes, in which rows are reference data and columns are classified data (K_{hat} = 0.72).

	Terrestrial marsh	Floating aquatic	Emergent aquatic	Open water	Forest	Total	Producer's accuracy (%)
Terrestrial marsh	321	10	2	1	8	342	93.8
Floating aquatic	0	36	0	0	0	36	100.0
Emergent aquatic	10	8	0	0	0	18	0.0
Open water	0	0	0	45	0	45	100.0
Forest	17	1	0	0	9	27	33.3
Total	348	55	2	46	17	468	
User's accuracy (%)	92.2	65.5	0.0	97.8	52.9		

Note: Emergent terrestrial and shrub class was merged with grasses–sedges class to form the terrestrial marsh class.

than those for either type alone, so they are discussed here. **Table 9** shows the adjusted R^2 (R^2_{adj}) values for the linear and logarithm-transformed models of total (aquatic + terrestrial) biomass stratified as all biomass (green + senescent), green biomass, and senescent biomass. Most linear models had poor fits and were therefore not analyzed further. Logarithm transformation of biomass (conducted for reasons given in the Methods) significantly improved the R^2_{adj} of two of the three models listed in **Table 9**.

For the total vegetation ((aquatic + terrestrial)/(green + senescent)) logarithm of biomass model, six variables were entered, which is adequate for predictive purposes given that the number of samples (75) was more than 10 times the number of variables in the model (Stevens, 1996). For the logarithm of green biomass model, the same six variables were entered, whereas for the logarithm of senescent biomass only one variable was entered, and the model was poorer than its corresponding linear model. Multicollinearity analysis of the two six-variable models showed that the NIR homogeneity texture (HOM5nir) was inversely correlated with the NIR standard deviation texture (STDEV5nir; r = –0.83) and was entered into the model after STDEV5nir. The VIF values for HOM5nir and STDEV5nir were 3.42 and 4.18, respectively, for both models, exceeding the calculated thresholds of 2.65 for the log(green + senescent biomass) model and 3.01 for the log(green biomass) model. In assessing model prediction in the following section, it was also found that models including both of these variables significantly overestimated biomass. HOM5nir was therefore dropped and both regressions were rerun. The VIF for these two models then fell to 2.57 and 2.56, respectively, and the models were no longer strongly biased. The results for the final multiple-variable model for log(green biomass), which was the best model produced, are listed in **Table 10** showing the R^2 contribution of each variable.

MN5grn texture was the first variable entered and dominated the variance accounted for in almost all models. It typically

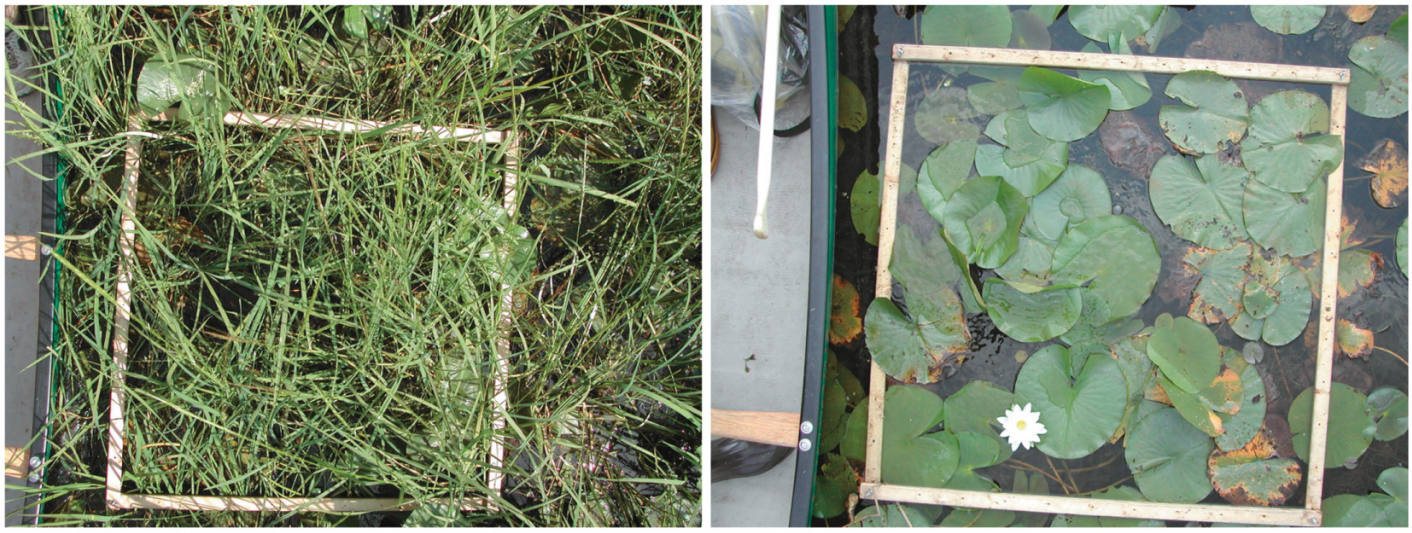

Figure 4. Aquatic vegetation showing differences in structure between (a) emergent aquatic plot with common reed (*Phragmites australis*) dominant and (b) floating aquatic plot with fragrant white water lily (*Nymphaea odorata*) dominant.

Table 8. Error matrix for five-class neural network 9 classification, in which rows contain number of pixels assigned as reference data and columns contain number of pixels assigned as classified data.

	TERm	FLAQ	EMAQ	OW	FOR	Row total	Producer's accuracy (%)
TERm	313	6	10	0	13	342	91.52
FLAQ	0	36	0	0	0	36	100.00
EMAQ	18	0	0	0	0	18	0.00
OW	1	0	0	44	0	45	97.78
FOR	21	4	0	0	2	27	7.41
Column total	353	46	10	44	15	468	
User's accuracy (%)	88.67	78.26	0.00	100.00	13.33		

Table 9. Adjusted R^2 (R^2_{adj}) for models of total combined biomass, total green biomass, and total senescent biomass in combined terrestrial and aquatic environments.

Y variable	R^2_{adj}
Total green and senescent biomass	0.257
Total green biomass	0.385
Total senescent biomass	0.183
Log(total green and senescent biomass)	0.623
Log(total green biomass)	0.639
Log(total senescent biomass)	0.069

accounted for about six to ten times the variance of any other subsequent variable entered. This texture measure is representative of the broader statistical group of texture measures (Hall-Beyer, 2007). It is the summed probabilities of all pairs of pixel values in the sample window multiplied by the respective reference pixel value in each pair. This multiplication results in increasing mean texture with increasing image brightness, and therefore this texture measure represents both overall spatial variation in image brightness and the image (spectral) brightness itself. As a result, it is usually highly correlated with the spectral band brightness from which it is derived. This point is expanded on in the Discussion section. The other variables entered into models included blue band brightness, the ASVI vegetation index, NIR mean texture (MN3nir), STDEV5nir, green GLDV angular second moment texture (GLA2M3grn), and HOM5nir. Although these variables made only minor contributions to the models, these results show that Ikonos image texture is generally more associated with modelling biomass of these wetlands than spectral data.

The best log(green biomass) model (Equation (1); **Table 10**) was applied to the Ikonos imagery to map green biomass, converting log(biomass) back to biomass in grams per square metre (**Figure 5**):

$$y = 5.863 - 0.269X_1 + 0.148X_2 - 0.244X_3 - 0.394X_4 - 1.979X_5 \quad (1)$$

where y is log(green biomass), X_1 is MN5grn, X_2 is MN3nir, X_3 is STDEV5nir, X_4 is GLA2M3grn, and X_5 is ASVI.

Table 10. R^2 contribution of independent variables in log(green biomass) model.

	R^2	R^2_{adj}	S_e	p	R^2 contribution
Log(green biomass) model	0.61	0.58	0.24; 1.73	<0.019	
Model variables					
MN5grn					0.431
MN3nir					0.043
STDEV5nir					0.051
GLA2M3grn					0.053
ASVI					0.032

Note: S_e is given in logarithm units followed by g/m^2.

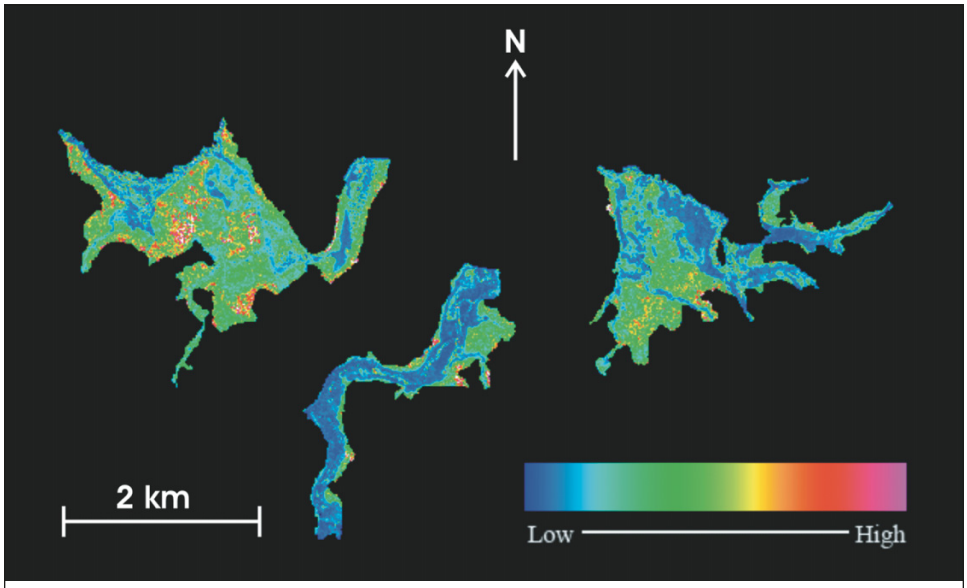

Figure 5. Map of predicted green biomass from regression Equation (1).

Table 11. Multiple-variable model validation results for five models, each using a random 70:30 model:validation split sample.

Validation	R^2	R^2_{adj}	S_e	p	Mean error (%)	Mean absolute error (%)	RMSE (%)
1	0.52	0.48	0.26; 1.82	0.026	–1.21	30.18	49.20
2	0.54	0.53	0.25; 1.78	0.000	–13.52	48.42	65.23
3	0.72	0.69	0.21; 1.62	0.020	–1.74	52.88	69.12
4	0.58	0.56	0.23; 1.70	0.001	–18.50	46.43	63.61
5	0.47	0.44	0.28; 1.91	0.011	–3.08	45.06	65.29
Avg.	0.57	0.54	0.25; 1.78	0.012	–7.61	44.59	62.49

Note: S_e is shown in logarithm units and g/m^2, and errors are expressed as percentages of the mean field-measured biomass.

Biomass model assessment and validation

Table 11 shows the results of validation of the log(green biomass) model (with HOM5nir excluded due to multicollinearity) using five additional stepwise regressions and random sets of training and validation data split 70:30 (i.e., 70% training and 30% validation). Errors are expressed as percentages of the mean field-measured biomass. The mean error for all models indicates moderate negative bias of 1%–18%, indicating that predicted biomass was always less than field-measured biomass. The mean absolute error and RMSE were quite high, with RMSE being more affected by outliers due to the use of squared differences between predicted and reference data. Based on the average mean absolute error of about 40% of the mean field-measured biomass, it was deemed appropriate to aggregate the map of **Figure 5** into three classes of biomass. **Figure 6** shows an example of three arbitrarily defined classes of low (0–1000 g/m^2), medium (1001–2000 g/m^2), and high (>2001 g/m^2) biomass. The visual pattern of biomass spatial distribution in this map corresponds well to the spatial distribution of biomass observed in the field, with lower biomass found in aquatic areas next to open water and higher biomass in terrestrial marsh areas. This is an example

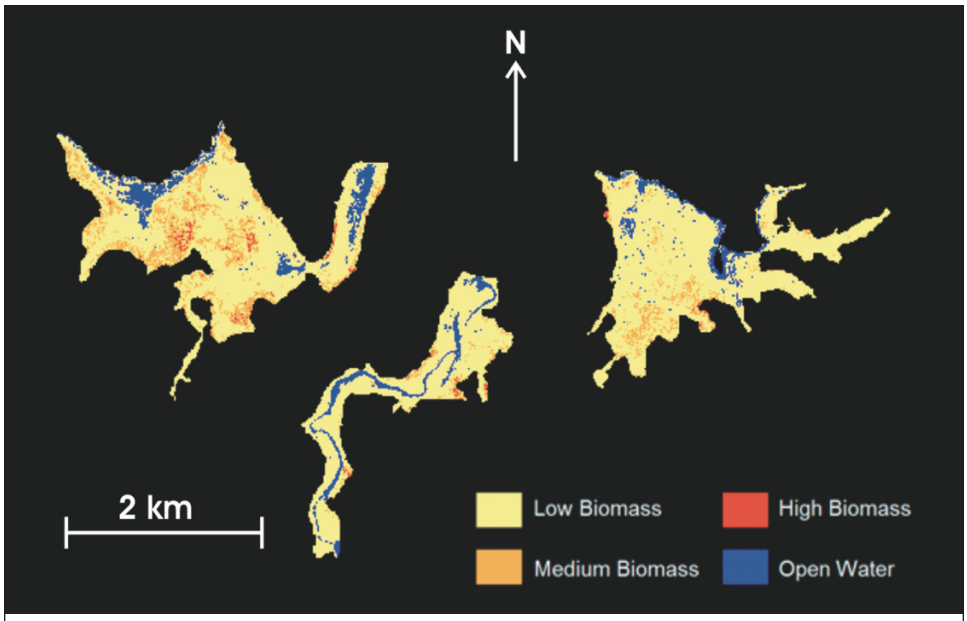

Figure 6. Green biomass aggregated to three levels from the results of **Figure 5**.

Table 12. Single-variable model validation results for five models, each using a random 70:30 model:validation split sample.

Model No.	R^2	R^2_{adj}	S_e	p	Mean error (%)	Mean absolute error (%)	RMSE (%)
1	0.34	0.33	0.30; 1.99	0.000	–11.17	37.81	56.09
2	0.54	0.53	0.25; 1.78	0.000	–13.52	48.42	65.23
3	0.42	0.40	0.28; 1.91	0.000	–5.15	40.88	54.46
4	0.40	0.39	0.27; 1.86	0.000	–14.97	39.64	53.87
5	0.33	0.32	0.31; 2.04	0.000	–10.22	34.31	42.83
Avg.	0.41	0.39	0.28; 1.91	0.000	–11.01	40.21	54.50

Note: MN5grn was entered for all models except model 2, where MN3grn was entered. S_e is shown in logarithm units and g/m^2, and errors are expressed as percentages of the mean field-measured biomass.

only; one could define other class boundaries, use nonlinear intervals, or use classes defined by ecological or management considerations.

Table 12 shows the results of the same type of validation as that given previously for five models but constrained to allow only one variable to enter. MN5grn was entered for four of the models, and MN3grn was entered for the other model. The mean error for all models again indicates moderate negative bias of 5%–14%. Despite lower model R^2 and higher S_e than the multiple-variable models of **Table 11**, the lower absolute error and RMSE of the single-variable models indicate that for predictive purposes the more complex model of Equation (1) was probably overfit and is not as useful for predictive purposes.

Discussion

Wetland vegetation classification

In this research, separability analyses provided a good starting method for selecting textures and determining which spectral–textural combinations should be used for classification. They also supported the merging of wetland classes that were found to be spectrally–texturally similar. From the separability analyses, a subgroup of variable sets was retained for classification tests. It should be noted that the ranking of these variable sets from separability analyses did not correspond exactly to the ranking based on classification accuracy. This may be because separability is calculated from the training data and represents a distance measure (inverse variance–covariance weighted) between means of training class pairs, whereas classification accuracy is calculated from a separate validation dataset and represents the capability for spatial extension and prediction using the training data.

Classification accuracy improved by 26.5%, after merging of confused classes and decreasing the class set from seven to five. Gluck et al. (1996) used Landsat TM imagery to map regional wetlands in northwestern Ontario and found that merging of spectrally similar wetland classes improved classification accuracy by about 10%. This research also found higher classification accuracy was achieved with the inclusion of image texture. Of the 12 textures evaluated, green band angular second moment and NIR band contrast, both using 5 × 5

windows, were found to best discriminate between class pairs. It is difficult to compare these results with those from previous studies because there is little in the literature on the evaluation of texture in wetland classification. In one study, however, Arzandeh and Wang (2002) also found these two texture measures to be useful in mapping marshes, although they found that a combination of four texture measures was better than two.

Of the vegetation indices evaluated, DVI, NDVI, and TVI were found to be useful for discriminating between different wetland vegetation types and improving classification accuracy relative to using spectral band combinations. From the literature surveyed, the only vegetation index based on visible and NIR bands that had been tested for wetland classification purposes was NDVI. Lee et al. (1992) used multispectral SPOT data to map coastal wetlands and found that from visual analysis NDVI appeared to best distinguish marsh types. In addition, Hunter and Power (2002) found that the inclusion of NDVI specifically increased classification accuracy, particularly for intertidal marsh classes. In this research, seven vegetation indices were compared. It was determined that NDVI and TVI, each in combination with the visible bands and two texture measures, produced five-class overall accuracies that were close to 88%, which was better than could be achieved by the spectral bands alone or by other vegetation index combinations.

To improve on the results found here, it may be possible to discriminate some of the merged classes if a different sensor is used (with a middle infrared or radar band), if phenological differences during the growing season could be analyzed with multidate imagery, or if a different classifier was used. An example of the latter would be hierarchical classification with given spectral and (or) texture measures used selectively to discriminate certain classes (perhaps in a decision-tree approach) instead of using them together in a single classification. In addition, object-based classification could be used independently or in a hierarchical manner. This would allow classification of spectral and spatial data for segmented objects, which has often been shown to improve classification accuracy and provide more meaningful map objects than pixel-based classifiers. Our current wetland research is taking this approach. Lastly, understanding the spatial characteristics of each class would benefit such classification procedures. The range of spatial dependence (from semivariogram analysis (Lévesque and King, 2003) or other measures of spatial scale such as lacunarity analysis (Butson and King, 2006)) could be used to define appropriate texture window sizes or to distinguish between classes that are spectrally similar.

A significant limitation of the classification methodology was the small sample sizes for the grasses–sedges, emergent aquatic, and shrub classes and small coverage of the field sample sites. This was due to an effort to distribute numbers of samples in a manner that was spatially representative of class occurrence and to minimize spatial autocorrelation in sampling. However, errors in these small sets of validation pixels were proportionally quite significant. In an alternative approach, if each class is considered equally important, approximately equal sample sizes for each class would be appropriate.

Biomass modelling

In repeated stepwise regression modelling, significant models of log(biomass) were produced, but the RMSE of separate validation data was close to 40% of the mean field-measured biomass. Consequently, the predicted values for all pixels were aggregated into three relative classes to produce a map of estimated biomass. Of interest was the fact that the models were dominated by the Mean co-occurrence texture measure, with other textures and only one vegetation index being minor predictors. Texture indicates radiance or reflectance variation in the window area in which it is calculated. In the models, increasing biomass was found to be associated with decreasing image texture. In the terrestrial areas where biomass was higher than that in all but a few aquatic plots, vegetation cover was greater, and there was no significant shadowing, image texture resulted from vegetation (types as given in **Table 1**) radiance and some soil radiance. Over the 12 m × 12 m window areas in which texture was extracted, the combined signal from these two cover types was not highly spatially variable, resulting in low to moderate image textures. However, in the aquatic areas vegetation radiance was interspersed to varying degrees with radiance from open water, which is very low in all bands, resulting in higher image textures. This was particularly evident in the floating aquatic class, which had lower biomass than most emergent aquatic plots and was dominated by flat leaves of lily pads interspersed with open water in patches of varying size. This relation of image texture to biomass, although indirect, was stronger than relations of biomass with any of the spectral bands or vegetation indices, resulting in models of biomass being comprised mostly of texture predictor variables.

It should be noted, however, that the mean green texture measure is highly correlated with green band brightness (r = 0.90), as mentioned in the Results. Thus, it is really representing a combination of spectral reflectance and overall spatial variability in the defined sample window. As a test, using the green spectral band alone produced a model of log(biomass) with slightly lower significance, R^2, and S_e than the average of the mean green texture models in **Table 12**. This shows that, given their commonality, in the stepwise regression procedure, once mean green texture was entered, green brightness could not significantly account for any remaining variance.

Due to practical constraints in this study, there were two positional aspects of the data used that could have limited better model development. First, plot positions and GCPs for image georeferencing were measured using a GPS with known specifications of submetre accuracy in differential mode, and the image georeferencing transformation error was shown to be about one-twentieth of a pixel (0.2 m). However, the combined error of these and the possible mismatch of pixel orientation with plot orientation may have resulted in some plot image data being extracted from pixels not exactly matching the field

sample locations. This error was not expected to exceed the 4 m multispectral pixel size for more than a few plots, but it may have affected biomass model quality. Second, image texture calculated from an area of 12 m × 12 m (3 × 3 pixels) encompassing each biomass sample location was found to be significantly related to biomass measured in a 1 m^2 area within the larger texture windows. This mismatch of sample area was unavoidable because it was not possible to clip biomass from larger areas and maintain adequate sample numbers. Clipping, breaking up, and bagging of all green and senescent biomass from seventy-five 1 m^2 sample areas followed by transport of the vegetation out of these extensive wetlands by canoe or on foot was a very difficult task. To compensate, significant effort was made to locate the biomass samples within areas that were visually very uniform in vegetation type over a minimum of 12 m × 12 m and usually much greater than this. Fifty-one of the 75 plots were known to be uniform over at least 12 m × 12 m. Plots with some mixing of vegetation classes within the 12 m × 12 m area surrounding a biomass sample plot included (*i*) emergent terrestrial and shrub classes (12 sample locations), and (*ii*) floating aquatic and emergent aquatic classes (7 sample locations). Small linear riparian wetland areas in Kilmarnock and Irish Creek suffered most from mixed vegetation within sample areas, whereas samples in larger areas of these wetlands and in Barbers Creek were very uniform in vegetation class. The significant relationship found between texture and biomass indicates that biomass spatial autocorrelation within the windows was high; however, the relationship may improve if biomass data could be measured or derived for larger areas at each sample location.

Previous studies have not modelled riparian biomass using high spatial resolution imagery such as Ikonos. However, some other studies of wetland productivity have been conducted using other sensors. Regression modelling of short and tall *Spartina alterniflora* biomass in a salt-marsh environment was conducted by Hardisky et al. (1984) using NDVI derived from simulated Landsat data. From all model evaluations they determined, as in this study, that live biomass was on average underestimated. The short population model ($n = 139$) achieved an R^2 of 0.43, a mean absolute error of 93 g/m^2, and an RMSE of 122 g/m^2. The tall population model ($n = 46$) achieved an R^2 of 0.71, a mean absolute error of 175 g/m^2, and an RMSE of 228 g/m^2. These error magnitudes are similar to those found in this study, although they could not be expressed as a percent relative to mean biomass due to a lack of reported data.

The regression method used in the study is commonly applied as a standard for comparison to other studies and because general knowledge of such methods is widespread. Future research could include further in-depth regression analysis, for example of stratification for biomass modelling within given classes such as the five to seven classes tested in the classification portion of this study, using land cover as an additional nominal variable in nonparametric modelling of biomass, and analysis of the impact of classification error on biomass estimates.

Conclusions

This study has shown that spatial heterogeneity of vegetation type and biomass within riparian wetlands can be mapped using high spatial resolution Ikonos imagery. These data and methods may improve the attribute detail over that which is obtained using current Ontario Wetland Evaluation System (OWES) field-based methodology of assigning single attributes to delineated wetlands. Thematic land-cover maps derived from satellite image classification techniques can aid in the analysis of spatial patterns and help identify wetland areas that are susceptible to developmental and agricultural pressures. These attributes are scored within the OWES and help to determine the relative value of a given wetland. Maps of land-cover type or biophysical parameters such as vegetation structure can also be used to analyze and monitor unevaluated or inaccessible wetlands or, if the spatial resolution is high enough, they can reveal spatial patterns within wetlands that cannot be easily assessed from the ground.

In this research three classes of wetland were successfully mapped using image texture and spectral information: terrestrial marsh, floating aquatic, and open water. The emergent aquatic class was consistently classified incorrectly, though the output map showed that its assigned pixels visually coincided with known general areas of occurrence of this class in the field. Forest pixels were consistently confused with terrestrial marsh vegetation in all classifications. For biomass modelling, a highly significant regression model was used to produce a map showing the continuous biomass gradient in each of the three wetlands. Biomass was then scaled to relative categories (low, medium, and high) because the mean absolute error in model validation was approximately 40%. The three-level estimated biomass map patterns corresponded well visually with the expected spatial distribution of lower biomass in the aquatic areas next to open water and higher biomass in the terrestrial marsh areas.

In classification of vegetation and water and in regression modelling of biomass, Ikonos image texture was found to be complementary to and generally more important than spectral information. Future research will concentrate on improving classifications and models with other spatial and temporal information, additional information types (e.g., 3 m RADARSAT-2 data), and better sampling methodology to improve sample sizes of less common classes. These will be integrated within a multiscale study of temporal monitoring of wetland change within and between growing seasons.

Acknowledgements

This research was funded by a Natural Sciences and Engineering Research Council of Canada (NSERC) grant to D. King. The authors are grateful to Scott Mitchell for advice throughout this project and to Ravinder Virk and Craig Dillabaugh for intensive assistance in the field and laboratory.

References

Allison, P.D. 1999. *Multiple regression: a primer.* Pine Forge Press, Thousand Oaks, Calif.

Arzandeh, S., and Wang, J. 2002. Texture evaluation of RADARSAT imagery for wetland mapping. *Canadian Journal of Remote Sensing*, Vol. 28, No. 5, pp. 653–666.

Austen, M.J., Cadman, M.D., and James, R.D. 1994. *Ontario birds at risk: status and conservation needs*. Federation of Ontario Naturalists, Toronto, Ont., and Long Point Bird Observatory, Long Point, Ont.

Bannari, A., Morin, D., and Bonn, F. 1995. A review of vegetation indices. *Remote Sensing Reviews*, Vol. 13, pp. 95–120.

Butson, C.R., and King, D.J. 2006. Lacunarity analysis to determine optimum extents for sample-based spatial information extraction from high-resolution forest imagery. *International Journal of Remote Sensing*, Vol. 27, pp. 105–120.

Congalton, R.G. 1991. A review of assessing the accuracy of classifications of remotely sensed data. *Remote Sensing of Environment*, Vol. 37, pp. 35–46.

Cronk, J.K., and Fennessy, M.S. 2001. *Wetland plants biology and ecology.* Lewis Publishers, Boca Raton, Fla.

Dechka, J.A., Franklin, S.E., Watmough, M.D., Bennett, R.P., and Ingstrup, D.W. 2002. Classification of wetland habitat and vegetation communities using multi-temporal Ikonos imagery in southern Saskatchewan. *Canadian Journal of Remote Sensing*, Vol. 28, pp. 679–685.

Eastwood, J.A., Yates, M.G., Thomson, A.G., and Fuller, R.M. 1997. The reliability of vegetation indices for monitoring saltmarsh vegetation cover. *International Journal of Remote Sensing*, Vol. 18, pp. 3901–3907.

Foody, G.M., Lucas, R.M., Curran, P.J., and Honzak, M. 1996. Estimation of the areal extent of land cover classes that only occur at a sub-pixel level. *Canadian Journal of Remote Sensing*, Vol. 22, pp. 428–432.

Freund, R.J., and Wilson, W.J. 1998. *Regression analysis: statistical modeling of a response variable*. Academic Press, San Diego, Calif.

Gerson, H. 1988. *Status report on the black tern,* Chlidonias niger*, in Canada*. Committee on the Status of Endangered Wildlife in Canada (COSEWIC), Ottawa, Ont. 56 pp.

Gluck, M., Rempel, R., and Uhlig, P.W.C. 1996. *An evaluation of remote sensing for regional wetland mapping applications*. Ontario Forest Research Institute, Sault Ste Marie, Ont. Forest Research Report 137.

Green, E.P., Clark, C.D., Mumby, P.J., Edwards, A.J., and Ellis, A.C. 1998. Remote sensing techniques for mangrove mapping. *International Journal of Remote Sensing*, Vol. 19, pp. 935–956.

Hall-Beyer, M. 2007. *The GLCM tutorial home page*. Available from www.fp.ucalgary.ca/mhallbey/tutorial.htm.

Hammer, D.A. 1997. *Creating freshwater wetlands*. 2nd ed. CRC Press Incorporated, Boca Raton, Fla.

Haralick, R.M., Shanmugan, K., and Dinstein, I. 1973. Textural features for image classification. *IEEE Transactions on Systems, Man and Cybernetics*, Vol. 3, No. 6, pp. 610–621.

Hardisky, M.A., Daiber, F.C., Roman, C.T., and Klemas, V. 1984. Remote sensing of biomass and annual net aerial primary productivity of a salt marsh. *Remote Sensing of Environment*, Vol. 16, pp. 91–106.

Herr, A.M., and Queen, L.P. 1993. Crane habitat evaluation using GIS and remote sensing. *Photogrammetric Engineering & Remote Sensing*, Vol. 59, pp. 1531–1538.

Heute, A.R. 1988. A soil-adjusted vegetation index. *Remote Sensing of Environment*, Vol. 25, pp. 295–309.

Hunter, E.L., and Power, C.H. 2002. An assessment of two classification methods for mapping Thames Estuary intertidal habitats using casi data. *International Journal of Remote Sensing*, Vol. 23, pp. 2989–3008.

Jensen, J.R. 2005. *Introductory digital image processing: a remote sensing perspective.* Prentice Hall Inc., Upper Saddle River, N.J.

Jensen, J.R., Christensen, E.J., and Sharitz, R. 1984. Nontidal wetland mapping in South Carolina using airborne multi-spectral scanner data. *Remote Sensing of Environment*, Vol. 16, pp. 1–12.

Kavzoglu, T., and Mather, P.M. 2003. The use of backpropagating artificial neural networks in land cover classification. *International Journal of Remote Sensing*, Vol. 24, pp. 4907–4938.

Larson, J.S., and Newton, R.B. 1981. *The value of wetlands to man and wildlife*. Department of Forestry and Wildlife Management, University of Massachusetts, Amherst, Mass., Cooperative Extension Service, University of Massachusetts, and US Department of Agriculture and County Extension Services Cooperating. Report SP-125.

Lee, J.K., Park, R.A., and Mausel, P.W. 1992. Application of geoprocessing and simulation modeling to estimate impacts of sea level rise on the northeast coast of Florida. *Photogrammetric Engineering & Remote Sensing*, Vol. 58, pp. 1579–1586.

Lévesque, J., and King, D.J. 2003. Spatial analysis of radiometric fractions from high-resolution multispectral imagery for modelling forest structure and health. *Remote Sensing of Environment*, Vol. 84, pp. 589–602.

Lewis, W.M., Jr. 2001. *Wetlands explained*: *wetland science, policy and politics in America*. Oxford University Press Incorporated, New York.

Lyon, J.G., and McCarthy, J. 1995. Introduction to wetland applications. In *Wetland and environmental applications of GIS*. Edited by J.G. Lyon and J. McCarthy. CRC Press Incorporated, Boca Raton, Fla. pp. 27–30.

Mitsch, W.M., and Gosselink, J.G. 2000. *Wetlands*. 3rd ed. John Wiley and Sons Incorporated, New York.

Olmanson, L.G., Bauer, M.E., and Brezonik, P.L. 2002. Aquatic vegetation surveys using high-resolution Ikonos imagery. In *Pecora 15/Land Satellite Information IV/ISPRS Commission I/FIEOS Conference Proceedings*, 10–15 November 2002, Denver, Colo. ISPRS Commission I, Paris. pp. 1–5.

OMNR. 1993. *Ontario Wetland Evaluation System, southern manual*. 3rd ed. North East Science and Technology, Ontario Ministry of Natural Resources (OMNR), Toronto, Ont. Report TM-002. 178 pp.

Ozesmi, S.L., and Bauer, M.E. 2002. Satellite remote sensing of wetlands. *Wetlands Ecology and Management*, Vol. 10, pp. 381–402.

PCI Geomatics. 2004. PCI Geomatics, Richmond Hill. Ont. Available from www.pcigeomatics.com [software help file].

Pierce, L.E., Sarabandi, K., and Ulaby, F.T. 1994. Application of an artificial neural network in canopy scattering inversion. *International Journal of Remote Sensing*, Vol. 15, pp. 3263–3270.

Rogers, A.S., and Kearney, M.S. 2003. Reducing signature variability in unmixing coastal marsh thematic mapper scenes using spectral indices. *International Journal of Remote Sensing*, Vol. 25, pp. 2317–2335.

Rosenfield, G.H., and Fitzpatrick-Lins, K. 1986. A coefficient of agreement as a measure of thematic classification accuracy. *Photogrammetric Engineering & Remote Sensing*, Vol. 52, pp. 223–227.

Rumelhart, D.E., Hinton, G.E., and Williams, R.J. 1986. Learning internal representations by error propagation. Parallel distributed processing: explorations in the microstructure of cognition. In *Foundations*. Edited by D.E. Rumelhart and J.L. McClelland. MIT Press, Cambridge, Mass. pp. 318–362.

Stevens, J.M. 1996. *Applied multivariate statistics for the social sciences*. 3rd ed. Lawrence Erlbaum Associates Publishers, Mahwah, N.J.

Tan, Q., Shao, Y., Yang, S., and Wei, Q. 2003. Wetland vegetation biomass estimation using Landsat-7 ETM+ data. In *IGARSS'03, Proceedings of International Geoscience and Remote Sensing Symposium*, 21–25 July 2003, Toulouse, France. IEEE, New York. Vol. 4, pp. 2629–2631.

Thomson, A.G., Huiskes, A., Cox, R., Wadsworth, R.A., and Boorman, L.A. 2004. Short-term vegetation succession and erosion identified by airborne remote sensing of Westerschelde Salt Marshes, the Netherlands. *International Journal of Remote Sensing*, Vol. 25, pp. 4151–4176.

Twolan-Strutt, L. 1995. *Wetlands and woodlots*. North American Wetlands Conservation Council Canada, Ottawa, Ont. Issues Paper 1995-1.

Williams, M. 1990. *Wetlands: a threatened landscape*. Basil Blackwell Ltd., Oxford, UK.